

# **Chemically Prepared $\text{Li}_{0.6}\text{FePO}_4$ Solid Solution as a Vehicle for Studying Phase Separation Kinetics in Li-ion Battery Materials**

Laurence Savignac<sup>a</sup>, John M. Griffin<sup>b,c\*</sup>, Steen B. Schougaard<sup>a\*</sup>

<sup>a</sup> NanoQAM and the department of chemistry, Université du Québec à Montréal, Case postale  
8888 Succ. Centre-ville, Montréal, Qc, Canada, H3C 3P8

<sup>b</sup> Department of Chemistry, Lancaster University, Lancaster, UK, LA1 4YB

<sup>c</sup> Materials Science Institute, Lancaster University, Lancaster, UK, LA1 4YB

E-mail addresses: schougaard.steen@uqam.ca (S. B. Schougaard), j.griffin@lancaster.ac.uk  
(J. M. Griffin)

Phone: 1 514-987-3000 ext. 3911

## ABSTRACT

The commercial success of LiFePO<sub>4</sub> in high power Li-ion batteries is strongly related to its unique ultra-high rate charge/discharge performance that permits full charge in less than a minute. Since Li<sub>1-x</sub>FePO<sub>4</sub> ( $0.05 \leq x \leq 0.95$ ) separates into two phases with poor electronic and ionic conduction, this raises questions regarding the structural dynamics of phase separation. In this paper the transformation of metastable solid-solution Li<sub>0.6</sub>FePO<sub>4</sub> into a phase separated material is studied by analysis of the local and bulk structure. <sup>6</sup>Li MAS NMR is used to probe the immediate environment where proximity to Fe<sup>3+</sup> results in a significant shift in resonance frequency. Conversely, time-resolved XRD measurements reveal the transformation kinetics at the unit-cell scale. The XRD showed no preferential relaxation along the *a*, *b* and *c* crystal axes, consistent with the absence of a phase boundary perpendicular to the fast diffusion *b* axis. Key to the analysis is the preparation of the solid solution which yields phase pure samples exhibiting no evidence of the thermodynamically stable LiFePO<sub>4</sub> or FePO<sub>4</sub> phases. Long term measurement indicated that after 263 days under argon atmosphere these samples still exhibited a solid solution fraction > 40%. However, in presence of electrolyte, phase separation is significantly more rapid. The results presented supports *Li et al.* model [*Nature Mater.* **2018**, *17*, 915] where vehicular lithium transport at the surface determines the rate of phase separation and offers a methodology for studying high energy density LiMPO<sub>4</sub> systems (M=transition metal) that currently are limited by poor high rate performance.

## 1. Introduction

Lithiated transition metal phosphates constitute some of the most promising candidates for high-rate and robust Li-ion battery cathodes due to their outstanding structural stability. One material of this class, lithium iron phosphate, initially presented by Padhi *et al.*<sup>4</sup>, is already a commercial product often used where high power and safety is required. Here, the strong P-O bond hampers oxygen gas evolution during cycling even under abuse conditions. This is one of the many motivations for studying the *olivine* phases as opposed to metal oxides. From a kinetic point of view, Kuss *et al.*<sup>1</sup> recently showed that the complete delithiation process of LiFePO<sub>4</sub> can take place in less than 10 s, even though the mechanism invoked a phase barrier between the *olivine* and *heterosite* crystal structures. Counterintuitively, this suggests that the movement of the phase boundaries does not limit the rate of lithium deintercalation in this type of material. Nonetheless, the phase transition process raises questions regarding reactions rates, as the deintercalation/intercalation process *via* a phase transition mechanism is expected to affect ionic and electronic transport. More importantly, this has implications for understanding the redox mechanisms of other novel high energy density materials such as LiMn<sub>y</sub>Fe<sub>1-y</sub>PO<sub>4</sub><sup>5</sup> or LiCoPO<sub>4</sub><sup>6</sup>, as the origin of their sluggish lithium insertion and deinsertion kinetics<sup>7-8</sup> is not fully understood.

The typical *electrochemical* insertion and deinsertion pathway found in Li<sub>1-x</sub>FePO<sub>4</sub> particles with sub- $\mu\text{m}$  diameter using “low” current densities<sup>9</sup> entails phase separation during the vast majority of the process ( $0.05 \leq x \leq 0.95$ ). As such, the (dis)charge curves provide a flat plateau according to Gibb's phase rule.<sup>10</sup> At higher rates, a second pathway presents itself which proceeds *via* the formation of a Li<sub>x</sub>FePO<sub>4</sub> solid solution (Figure 1). This solid solution has an intermediate structure between LiFePO<sub>4</sub> and FePO<sub>4</sub> with uniformly distributed Li<sup>+</sup>. Given that the Li<sub>x</sub>FePO<sub>4</sub> solid solution is metastable at room temperature<sup>11-12</sup> only a few experimental studies are available. Of these, some focus on the particle level using *ex situ*

transmission electron microscopy<sup>13</sup> and *operando* high resolution microscopy<sup>14-16</sup>. In this context, the most important conclusions from these studies are that the redox reaction leads to formation of phase domains<sup>17</sup> with strong variations in lithium composition. The suggested origin of these heterogeneities include intraparticle dislocations<sup>18</sup> or variations in the carbon coating and defects at the surface<sup>19</sup>. In addition, at the electrode scale, *operando* X-ray techniques have been employed to show the presence of a solid solution phase at high (dis)charge rates.<sup>2, 20-21</sup> Importantly, features like particle size<sup>22</sup> and the ionic/electronic transport in the immediate environment surrounding particles<sup>3</sup> appear to strongly affect the reaction pathway.

In this work, we present an experimental approach for studying the phase transition process by taking advantage of the solid solution metastability. The aim is to clarify how the phase transition proceeds, as well as, examine which factors may affect its rate. By heat treating  $\text{Li}_{0.6}\text{FePO}_4$  (labeled LFP-2P, Figure 1) the solid solution (labeled LFP-SS) characterized by a single unit cell and uniformly distributed  $\text{Li}^+$  is formed<sup>23</sup>. This metastable structure is conserved at room temperature by rapid cooling.<sup>11</sup> Because relaxation to the two-phase structure at room temperature and under inert conditions is slow compared to the electrochemical process, techniques that require hours of sampling time can be employed using this approach. Additionally, in here, comparisons made under different storage conditions, are used to elucidate factors affecting the relaxation kinetics of the structure. To this end, MAS NMR spectroscopy is used as a local structural probe, while X-Ray diffraction (XRD) is used to determine larger scale effects, thereby providing a structural description of the relaxation of the metastable LFP-SS.

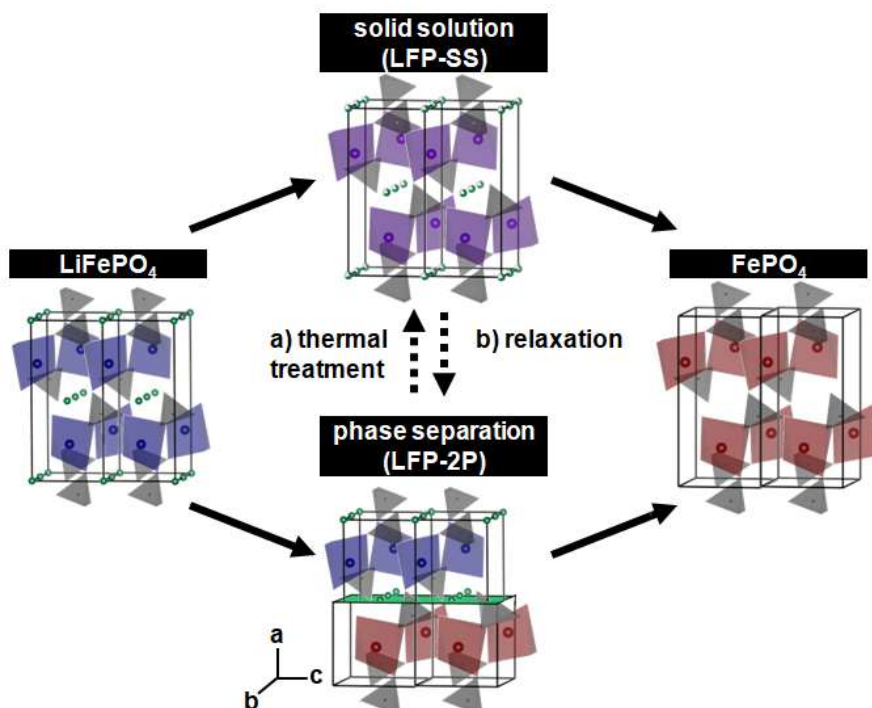


**Figure 1.** Scheme illustrating the solid solution (top) and the two phase (bottom) pathways for  $\text{LiFePO}_4$  delithiation and the relationship between two partially lithiated samples: a) the transformation from the ambient temperature thermodynamically stable two phase system to the solid solution b) the relaxation back to two phases.

## 2. Experimental Section

Carbon coated  $\text{LiFePO}_4$  (c- $\text{LiFePO}_4$ ) was obtained from Johnson Matthey Battery Materials. Complete chemical delithiation of the material was achieved by reacting 10 g of c- $\text{LiFePO}_4$  with 50 mL of hydrogen peroxide (ACS Grade 29.0-32.0%, EMD Chemicals) and 50 mL of glacial acetic acid (Alfa Aesar) in 300 mL nanopure water while stirring for 12h. The powder was recovered by centrifugation at 4000 rpm, followed by washing with 400 mL of nanopure water before drying overnight at  $80^\circ\text{C}$  in vacuum. The carbon coating of the resulting  $\text{FePO}_4$  was removed by heating at  $550^\circ\text{C}$  under air for 6h.<sup>23</sup> Specific lithium concentrations, *i.e.*  $x$  in  $\text{Li}_x\text{FePO}_4$ , were obtained by reacting with  $3x/2$   $\text{LiI}$  (Alfa Aesar 99%) per 1  $\text{FePO}_4$  unit suspended in acetonitrile (ACN - Aldrich 99.9%).<sup>23</sup> *E.g.* 8 g of  $\text{FePO}_4$  was added to 800 mL of 8 M  $\text{LiI}$  in ACN in a round bottom flask, and stirred for 24h. The resulting powder was

filtered on a Buchner funnel under vacuum, washed with 100 mL ACN and dried overnight at 80°C in vacuum.

Caution: The following procedure involves high temperature and risk of thermal shock. To obtain the solid solution, 1.5 g of  $\text{Li}_{0.6}\text{FePO}_4$  was heated in a glass crucible in a tubular oven (MTI Corporation, GSL-1300-40X) under  $\text{N}_{2(\text{g})}$  at 500°C for 15h. The powder sample was removed from the oven and *immediately* poured, still in its glass crucible, into a  $\text{N}_{2(\text{l})}$  filled plastic container. Subsequently, this container was connected to a vacuum system to prevent contact with air/humidity while  $\text{N}_{2(\text{l})}$  was removed by evaporation. The evacuated  $\text{N}_2$  free setup was entered into an  $\text{Ar}_{(\text{g})}$  filled glovebox (water and  $\text{O}_2$  content < 1ppm) for sample storage. For samples exposed to electrolyte, 0.06 g of  $\text{Li}_{0.6}\text{FePO}_4$  was placed in a 2 mL vial filled with 1M  $\text{LiPF}_6$  in EC:DMC (1:1) (BASF). Immediately prior to analysis, samples were filtered, rinsed with 1 mL of anhydrous ACN (Aldrich 99.8%) and dried under vacuum for 10 min.

The Li content of samples was confirmed by atomic emission spectroscopy (AES) where 9 mg of  $\text{Li}_{0.6}\text{FePO}_4$  was dissolved in 20 mL boiling concentrated nitric acid (Caledon), transferred in a 100 mL volumetric flask and subsequently diluted 10/100 mL in 5%  $\text{HNO}_3$ . A calibration curve (0.1 to 0.6 ppm) was made from Li standard solution (Alfa Aesar,  $\text{Li}_2\text{CO}_3$  in 5%  $\text{HNO}_3$ ) and measurements performed on a Varian SpectrAA 220 FS at 670.8 nm. Particle morphology was examined using a JEOL JSM840 scanning electron microscope (SEM), a SEI detector and 15.0 kV acceleration voltage. Samples were coated with a thin gold layer prior to analysis. Ambient temperature  $^6\text{Li}$  MAS NMR was recorded with a 400 MHz Bruker Avance III HD WB spectrometer and a 9.4T magnetic field strength. Experiments were performed using a Bruker 3.2 mm probe at a MAS rate of 20 kHz. Spectra were referenced relative to 1M  $\text{LiCl}$  solution (0 ppm). A Hahn echo pulse sequence was used with the echo delay synchronized to one rotor period (50  $\mu\text{s}$ ). The 90° pulse length was 4  $\mu\text{s}$  and a recycle

delay of 0.2 s was used. For the kinetic experiment only (Figure S-3), a 1.9 mm probe at a MAS rate of 33.33 kHz was used with a 90° pulse length of 2.5 μs.

XRD was performed on a Bruker (D8 Advance) diffractometer, using a Cu K<sub>α</sub> (1.5418 Å) radiation. The voltage and the current used were 20 kV and 5 mA respectively. Diffractograms were recorded in the 2θ=15-70° range with a step size of 0.018 s<sup>-1</sup>. In order to provide an internal angle standard 11 m/m-% of silicon powder 1-5 μm (Alfa Aesar 99.5 %) was mixed with the sample through grinding. Rietveld refinement was executed on each sample refining respectively Li<sub>0.6</sub>FePO<sub>4</sub>, LiFePO<sub>4</sub> and FePO<sub>4</sub> phases in this order using Fullprof software<sup>24</sup>, details are available in Section 2 of the supporting information.

### 3. Results and Discussion

The sample preparation process (Figure 1a) entails that ambient temperature thermodynamically-stable two-phase structure (labeled LFP-2P) is heat treated to form a solid solution structure (labeled LFP-SS) characterized by a single unit cell and uniformly distributed Li<sup>+</sup>. This solid solution phase is maintained at room temperature by rapid cooling. The thermal shock experienced during preparation of the solid solution (~700°C/s) may affect the morphology. Given the importance of particle size and shape on the surface-to-volume ratio, which in-turn may affect the phase transition rate and pathway<sup>22</sup>, the morphology before and after formation of the solid solution was examined by SEM (Figure 2). The micrographs show no features that can distinguish the materials before and after quenching. The particle size is therefore not affected by the rapid cooling.

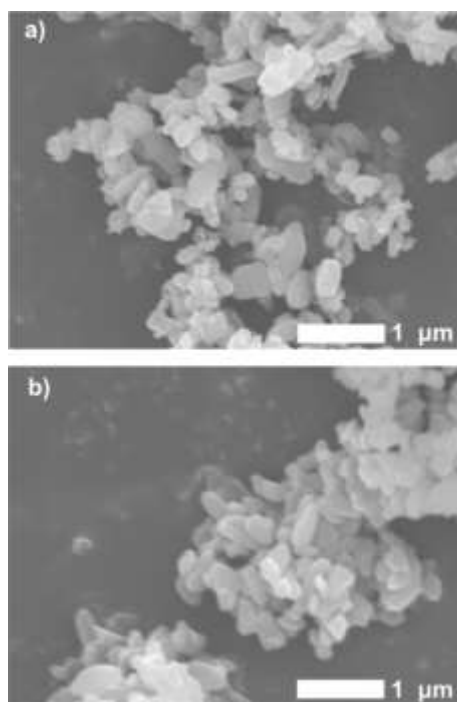


**Figure 2.** SEM micrographs of particles with 23,000x magnification for a) the LiFePO<sub>4</sub> starting material and b) LFP-SS.

With the aim of probing distinctive Li<sup>+</sup> environments in Li<sub>0.6</sub>FePO<sub>4</sub>, <sup>6</sup>Li MAS NMR spectroscopy was carried out on pristine LiFePO<sub>4</sub>, LFP-2P and LFP-SS samples. <sup>6</sup>Li was selected for NMR owing to the weaker dipolar coupling compared to <sup>7</sup>Li, leading to a sharper signal. The crystal structure of *olivine* LiFePO<sub>4</sub> adopts an orthorhombic space group where Li<sup>+</sup> is located at an inversion point, and the first coordination sphere is made up of three pairs of O linked to Fe<sup>2+</sup>. The <sup>6</sup>Li MAS NMR spectrum of pristine LiFePO<sub>4</sub> (Figure 3a) shows a single peak with a chemical shift of -52 ppm, consistent with the single crystallographic Li site and in agreement with previous studies<sup>25</sup>. Conversely, the LFP-2P sample (Figure 3b), where a Li<sup>+</sup> content of 0.629 ± 0.005 was confirmed by AES, exhibit a <sup>6</sup>Li spectrum with a single peak appearing at -58 ppm. The fact that the chemical shift is similar to the pristine material is consistent with the two-phase structure, where the local environment of Li<sup>+</sup> is expected to be very similar to the pristine material. In fact, the small -6 ppm difference is easily explained by for example defects modifying Li-O-Fe<sup>2+</sup> bond angles<sup>26</sup>. In addition, it could also be relate to an external phase effect, where Fe<sup>3+</sup> in the delithiated component

shields the magnetic field. This later effect was investigated by physically mixing different ratios of  $\text{LiFePO}_4$  and  $\text{FePO}_4$  to yield samples where an additional negative shift of up to 3 ppm could be associated with addition of paramagnetic  $\text{FePO}_4$  (supporting information, Figure S-1).

For the LFP-SS sample an asymmetric peak is observed centered around -12 ppm (Figure 3c). The asymmetry of the peak was examined *via* a two peak fitting process, using DMfit software<sup>27</sup> (complete LFP-SS fit is available in supporting information Figure S-2). The associated chemical shifts at +58 and -30 ppm, suggest the presence of  $\text{Li}^+$  nuclei situated within environments rich in  $\text{Fe}^{3+}$  and in  $\text{Fe}^{2+}$  respectively. This this assignment is based on fact that the  $\text{Fe}^{3+} t_{2g}^3 e_g^2$  spin configuration induces a stronger spin density transfer to  $\text{Li}^+$  (directly or *via* O) than the  $t_{2g}^3 e_g^1$  configuration of  $\text{Fe}^{2+}$ , thereby causing a stronger paramagnetic increase of the chemical shift<sup>26, 28-29</sup>. We note that the limited resolution does not allow for an unambiguous fit, the spectrum could also be consistent with a continuous distribution between these extreme peak positions, suggesting a range of different local  $\text{Fe}^{2+}/\text{Fe}^{3+}$  combinations affecting the  $^6\text{Li}$  signal.

As shown LFP-2P and LFP-SS samples, despite having the same atomic compositions, exhibit major differences for both peak shape and chemical shift. To probe their interrelation,  $^6\text{Li}$  MAS NMR spectra were recorded for LFP-SS samples over a period and of 7 day (Supporting information S-3) and after a relaxation period of 102 days (Figure 3d). This later sample shows a peak shape where intensity of the +58 ppm feature is reduced and the centre of gravity is shifted to -31 ppm, consistent with loss of the solid solution component as the sample relaxes to the two-phase structure containing  $\text{LiFe}^{2+}\text{PO}_4$  and  $\text{Fe}^{3+}\text{PO}_4$ . The overall conclusion from the NMR is that local environment for  $\text{Li}^+$  in LFP-SS is clearly distinct from LFP-2P. Moreover, no peaks were found outside the anticipated paramagnetic region, confirming that the observed features are not related to diamagnetic impurities.

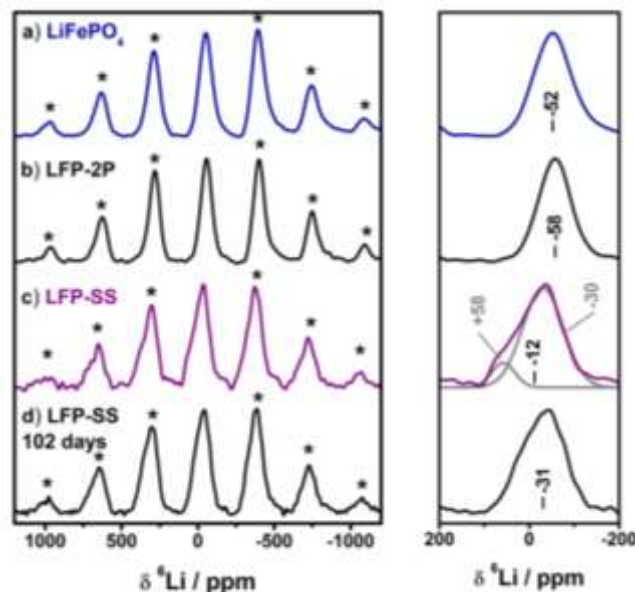


**Figure 3.**  ${}^6\text{Li}$  MAS NMR spectra of a)  $\text{LiFePO}_4$  starting material, b) LFP-2P and c) LFP-SS and d) LFP-SS after 102 days of relaxation where spinning sidebands are marked with asterisks. On the right the close up includes the position of the gravity center. For LFP-SS, peaks from the deconvolution and their chemical shifts are specified in grey.

To probe the bulk structural changes occurring during the phase separation, powder XRD was employed. Experiments were carried out under  $\text{Ar}_{(\text{g})}$  atmosphere to limit any undesirable surface reaction. The first diffractogram (Figure 4) was acquired few minutes after the quenching procedure, showing characteristic peaks of a single phase. This phase, denoted LFP-SS, has the (200) reflection located between the equivalent reflections of the  $\text{LiFePO}_4$  and  $\text{FePO}_4$  references. As time elapses two phases corresponding to the *olivine*  $\text{LiFePO}_4$  and *heterosite*  $\text{FePO}_4$  emerge, e.g. after 6 days these are visible as additional (200), (210) and (020)(211) reflection. Due to overlap of the (020) and (211) peaks the intensity of (200) vs (020) reflections does not reflect preferential kinetics of relaxation in the *a* vs *b* axes. Diffractograms of starting materials  $\text{LiFePO}_4$ ,  $\text{FePO}_4$  and LFP-2P are available in the supporting information (Figure S-5).

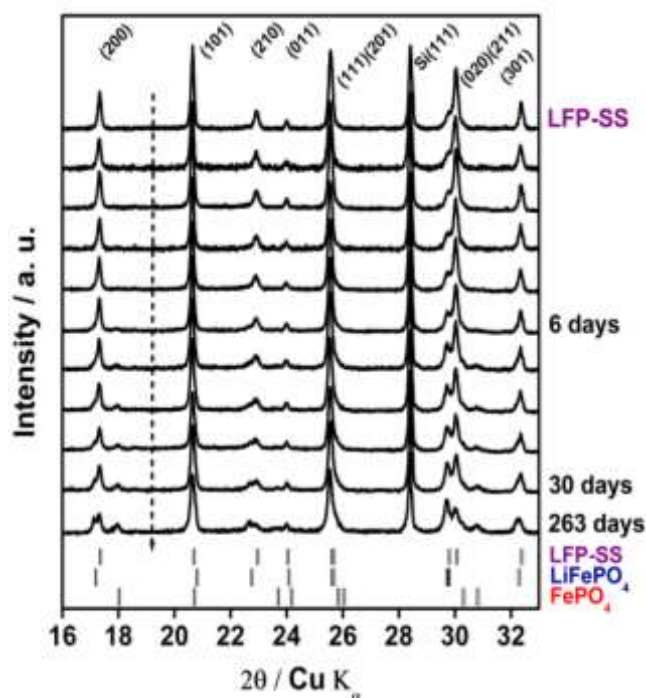


**Figure 4.** Diffractograms of LFP-SS and its timed resolved evolution from top to bottom and corresponding LFP-SS,  $\text{LiFePO}_4$  and  $\text{FePO}_4$ . Miller indexing from <sup>30</sup>.

In order to evaluate the kinetic profile for phase separation starting from  $\text{Li}_{0.6}\text{FePO}_4$ , Rietveld refinement was carried out, by varying the phase fraction (%) of three distinct structures, LFP-SS,  $\text{LiFePO}_4$  and  $\text{FePO}_4$  (Figure 4). The kinetic profile (Figure 5a) shows a decrease in the solid solution phase fraction, accompanied by formation  $\text{LiFePO}_4$  and  $\text{FePO}_4$  domain, as expected. Surprisingly, after 263 days of relaxation, 44% of the structure still is composed of solid solution.

In addition to providing phase separation kinetics (Figure 5a), the XRD was investigated to determine if a mechanistic model of  $\text{Li}^+$  transport during phase separation could be obtained. To this end, the unit cell parameters extracted from the Rietveld refinement of the different phases are examined as a function of time (Figure 5b-d). The initial solid solution phase shows relaxation into two phases, after an initial latency period of 3 days. This period may originate from the fact that the formation of the *heterosite* phase requires nucleation, thus possibly delaying its formation. After 20 days, the  $\text{LiFePO}_4$  and  $\text{FePO}_4$  phase unit cells

appear to have reached a stable size, in spite of the fact that 80% of the sample is still in the solid solution phase. This is further confirmed by the sample measured 263 days after the quenching process, where  $\text{LiFePO}_4$  and  $\text{FePO}_4$  phases are in the fully relaxed state.

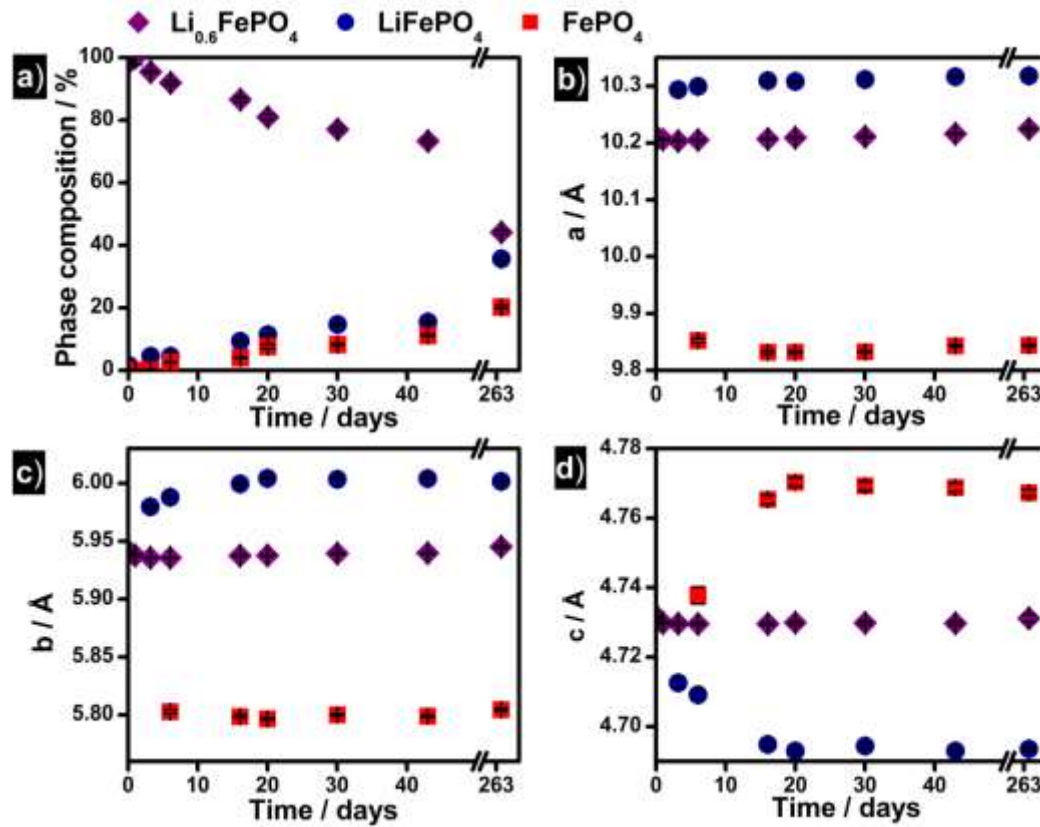


**Figure 5.** a) Kinetic profile of quenched  $\text{Li}_{0.6}\text{FePO}_4$  where phase's compositions and confidence intervals are extracted from Rietveld refinement. b-d) Unit cell parameters of LFP-SS,  $\text{LiFePO}_4$  and  $\text{FePO}_4$  their timed resolved evolution extracted from Rietveld refinement.

How  $\text{Li}^+$  move from LFP-SS to form  $\text{LiFePO}_4/\text{FePO}_4$  phases has been the subject of experimental<sup>3, 13, 31</sup> and theoretical investigations<sup>32-34</sup>. As  $\text{Li}^+$  transport occurs effectively only in one-dimensional  $b$  oriented channels, the internal phase separation mechanism would lead to formation of an interface perpendicular to this axis *i.e.* in the  $ac$  plane. With a diffusion coefficient of  $\sim 10^{-12} \text{ cm}^2 \text{ s}^{-1}$ <sup>35</sup> the calculated average diffusion distance exceeds the particle size within the first hour following the quench. However, we find no evidence of solid-solution unit-cell relaxation such as peak widening consistent with a steep concentration

gradient *i.e.* phase barrier perpendicular to the *b* axis. It is in this context important that the analysis is made from a phase pure sample, so that any concerns regarding epitaxial effects of residual LiFePO<sub>4</sub>/FePO<sub>4</sub> can be laid to rest. Overall, it appears that spinodal decomposition is not observed, when the displacement freedom of Li<sup>+</sup> is only in the *b* direction. This is not entirely unexpected as the large LiFePO<sub>4</sub>/FePO<sub>4</sub> mismatch in the *a* direction (supporting information Table S-1) should result in a large energy barrier to accommodate the unit cell modification parallel with this axis.

Since the solid solution given enough time will separate into two phases (figure 5a), the challenge is to explain the transport of lithium between the *b* axis channels. Here, three pathways are envisioned:

i) *Interparticle transport*. The lithium from one particle is transported out of the particle and into an adjacent particle, thereby lowering the energy of the system. In comparison with other studies using electrochemistry to prepare the solid solution, the method employed here does not expose the solid solution phase to ionic conducting liquids. This transport mechanism is therefore highly unlikely.

ii) *Intraparticle transport*. Li<sup>+</sup> and vacancies are transported between adjacent channels through the bulk of the structure, leading to increased relaxation kinetics<sup>3</sup>. This transport would be affected by the presence of Li-Fe antisite defects, which is suggested to provide an out-of-channel diffusion coefficient in the order of 10<sup>-16</sup> cm<sup>2</sup> s<sup>-1</sup><sup>36</sup>, sufficient to yield average diffusion distances in excess of the particle size within days. The chemical route used here leads to almost complete Li<sup>+</sup> removal in the initial step (For Li<sub>x</sub>FePO<sub>4</sub>, x=0.02 ± 0.005 by AA) (supporting information Figure S-5), therefore we expect no more than 2% defects in our sample<sup>37</sup>. Even with this low defect concentration, in our samples this mechanism cannot be ruled out.

iii) *Surface transport*.  $\text{Li}^+$  and vacancies are transported between adjacent channels over the surface. This requires diffusion to the surface, transport over the surface and reinsertion into channels. Presumably, *b* axis channels *close* to the phase barrier would be filled and emptied on the  $\text{LiFePO}_4$  and the  $\text{FePO}_4$  side respectively first, whereas a longer diffusion path and therefore more time would be required for channels at larger distance from the barrier. This is consistent with the observation that phase separation slows with time (figure 5a).

The method of sample preparation is of importance here. The chemical pathway used to reach a specific lithium composition ensures a uniform chemical potential around each particle, eliminating concerns that the point contact of the standard composited electrochemical electrode causes a heterogeneous concentration of lithium within the particle and between particles<sup>38</sup>. Moreover, as the surface is only exposed to inert gasses during preparation and storage, this type of sample is uniquely suited to isolate factors from the Li-ion battery chemistry that affects the phase separation process. To this end, the role of surface-electrolyte interface for commercial uncoated quenched material preserved in 1M  $\text{LiPF}_6$  in EC:DMC (1:1) was compared to the solid solution sample stored under  $\text{Ar}_{(g)}$ . The contrast between these two samples is clear after 6 days (Figure 6), since  $\text{LiFePO}_4$  and  $\text{FePO}_4$  XRD reflections are prominent only in the electrolyte stored sample. This highlights the role of surface interactions in the rate of phase separation, *i.e.* mechanism iii). Moreover, it highlights the importance of comparing results from electrochemical studies with data from “solvent free” samples, as the electrolyte environment is expected to strongly favour phase separation. From a kinetic point of view, this observation reiterates the critical role of  $\text{Li}^+$  ion concentration gradients in the electrolyte, solvent-particles surface tension, volume/surface ratio and importantly, the nature of the particle coating, in the charge storage mechanism of this type of phase transition materials.

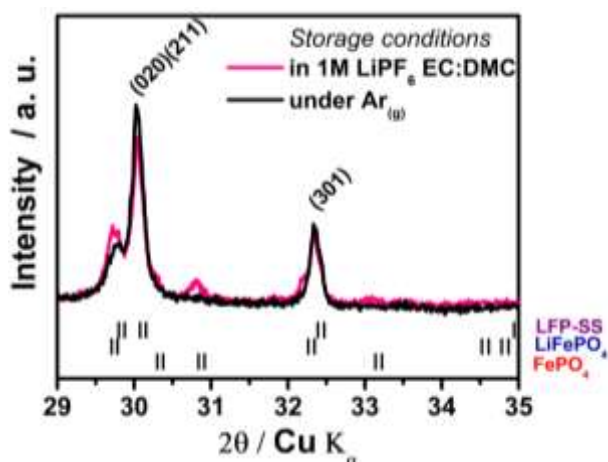


**Figure 6.** Comparative diffractograms of quenched  $\text{Li}_{0.6}\text{FePO}_4$  after 6 days with specific storage conditions and corresponding LFP-SS,  $\text{LiFePO}_4$  and  $\text{FePO}_4$ . Miller indexing from<sup>30</sup>.

#### 4. Conclusion

Phase pure solid solution samples of  $\text{Li}_{0.6}\text{FePO}_4$  were examined to provide insight into the phase separation mechanism.  $^6\text{Li}$  MAS NMR showed as expected a solid solution with mixed  $\text{Fe}^{3+}$  and  $\text{Fe}^{2+}$  interacting with  $^6\text{Li}$  through oxygen, which is distinctly different from the  $\text{Fe}^{2+}$ -O environment of  $\text{LiFePO}_4$ . XRD measurement showed the phase separation process to be remarkably slow, with solid solution phase fractions in excess of 40% persisting after six months. Moreover analysis of the solid solution XRD peaks vs. time shows the unit cell relaxing with the same absolute rate along all axes.

By using a chemical rather than electrochemical method of producing the solid solution phase, we were able to eliminate concerns regarding non uniform current distribution causing local concentration gradients both intra and interparticle, possibly inducing premature phase separation and/or bimodal distribution of lithium over the particle population.

Combined, this work provides independent confirmation of the “over-the-top” model developed *Li et al.*<sup>3</sup> where lithium diffusion between *b*-channel lithium is slow, but diffusion to the surface combined with vehicular surface transport and reinsertion into the structure on the other side of a phase barrier parallel with the *b*-axis is comparatively fast.

This mode of structural relaxation is highly important. Its presence in other promising transition metal phosphates like  $\text{LiMPO}_4$  (M=Mn, Co, Ni), would offer a design target for suppressing phase separation and thus maintain the solid-solution structure believed to provide superior ionic and electronic conductivity. As such, it offers hope for improving the charge/discharge kinetics so that the theoretical high energy density and safety of these materials can be harvested for practical use.

## Acknowledgements

The authors thankfully acknowledge the Natural Sciences and Engineering Research Council of Canada (NSERC) Grant RGPIN-2019-07200 for financial support. NMR measurements were completed as part of the International Internship program, thanks to the *Centre québécois sur les matériaux fonctionnels/Québec Centre for Advanced Materials* (CQMF/QCAM) as well as the *Fonds de recherche du Québec - Nature et les technologies* (FRQNT).

## Supporting Information

The supporting information is available for complementary results about  $^6\text{Li}$  MAS NMR, XRD and unit cell parameters relaxation.

## References

1. Kuss, C.; Trinh, N. D.; Andjelic, S.; Saulnier, M.; Dufresne, E. M.; Liang, G.; Schougaard, S. B., Structural Transformation of  $\text{LiFePO}_4$  during Ultrafast Delithiation. *The Journal of Physical Chemistry Letters* **2017**, 8 (24), 6160-6164.

2. Liu, H.; Strobridge, F. C.; Borkiewicz, O. J.; Wiaderek, K. M.; Chapman, K. W.; Chupas, P. J.; Grey, C. P., Capturing metastable structures during high-rate cycling of LiFePO<sub>4</sub> nanoparticle electrodes. *Science* **2014**, *344* (6191), 1252817.
3. Li, Y.; Chen, H.; Lim, K.; Deng, H. D.; Lim, J.; Fraggedakis, D.; Attia, P. M.; Lee, S. C.; Jin, N.; Moškon, J.; Guan, Z.; Gent, W. E.; Hong, J.; Yu, Y.-S.; Gabersček, M.; Islam, M. S.; Bazant, M. Z.; Chueh, W. C., Fluid-enhanced surface diffusion controls intraparticle phase transformations. *Nature Materials* **2018**, *17* (10), 915-922.
4. Padhi, A. K.; Nanjundaswamy, K. S.; Goodenough, J. B., Phospho-olivines as Positive-Electrode Materials for Rechargeable Lithium Batteries. *Journal of The Electrochemical Society* **1997**, *144* (4), 1188-1194.
5. Kobayashi, G.; Yamada, A.; Nishimura, S.-i.; Kanno, R.; Kobayashi, Y.; Seki, S.; Ohno, Y.; Miyashiro, H., Shift of redox potential and kinetics in Li<sub>x</sub>(Mn<sub>y</sub>Fe<sub>1-y</sub>)PO<sub>4</sub>. *Journal of Power Sources* **2009**, *189* (1), 397-401.
6. Liu, D.; Zhu, W.; Kim, C.; Cho, M.; Guerfi, A.; Delp, S. A.; Allen, J. L.; Jow, T. R.; Zaghbi, K., High-energy lithium-ion battery using substituted LiCoPO<sub>4</sub>: From coin type to 1 Ah cell. *Journal of Power Sources* **2018**, *388*, 52-56.
7. Yonemura, M.; Yamada, A.; Takei, Y.; Sonoyama, N.; Kanno, R., Comparative Kinetic Study of Olivine Li<sub>x</sub>MPO<sub>4</sub> ( M = Fe , Mn). *Journal of The Electrochemical Society* **2004**, *151* (9), A1352-A1356.
8. Bramnik, N. N.; Nikolowski, K.; Baetz, C.; Bramnik, K. G.; Ehrenberg, H., Phase Transitions Occurring upon Lithium Insertion–Extraction of LiCoPO<sub>4</sub>. *Chemistry of Materials* **2007**, *19* (4), 908-915.
9. Zhang, W.-J., Structure and performance of LiFePO<sub>4</sub> cathode materials: A review. *Journal of Power Sources* **2011**, *196* (6), 2962-2970.
10. Malik, R.; Abdellahi, A.; Ceder, G., A Critical Review of the Li Insertion Mechanisms in LiFePO<sub>4</sub> Electrodes. *Journal of The Electrochemical Society* **2013**, *160* (5), A3179-A3197.
11. Dodd, J. L.; Yazami, R.; Fultz, B., Phase Diagram of Li<sub>x</sub>FePO<sub>4</sub>. *Electrochemical and Solid-State Letters* **2006**, *9* (3), A151-A155.
12. Delacourt, C.; Poizot, P.; Tarascon, J.-M.; Masquelier, C., The existence of a temperature-driven solid solution in Li<sub>x</sub>FePO<sub>4</sub> for 0 ≤ x ≤ 1. *Nature Materials* **2005**, *4* (3), 254-260.
13. Chen, G.; Song, X.; Richardson, T. J., Electron Microscopy Study of the LiFePO<sub>4</sub> to FePO<sub>4</sub> Phase Transition. *Electrochemical and Solid-State Letters* **2006**, *9* (6), A295-A298.

14. Lim, J.; Li, Y.; Alsem, D. H.; So, H.; Lee, S. C.; Bai, P.; Cogswell, D. A.; Liu, X.; Jin, N.; Yu, Y.-s.; Salmon, N. J.; Shapiro, D. A.; Bazant, M. Z.; Tyliszczak, T.; Chueh, W. C., Origin and hysteresis of lithium compositional spatiodynamics within battery primary particles. *Science* **2016**, *353* (6299), 566-571.
15. Zhang, W.; Yu, H.-C.; Wu, L.; Liu, H.; Abdellahi, A.; Qiu, B.; Bai, J.; Orvananos, B.; Strobridge, F. C.; Zhou, X.; Liu, Z.; Ceder, G.; Zhu, Y.; Thornton, K.; Grey, C. P.; Wang, F., Localized concentration reversal of lithium during intercalation into nanoparticles. *Science Advances* **2018**, *4* (1), eaao2608.
16. Niu, J.; Kushima, A.; Qian, X.; Qi, L.; Xiang, K.; Chiang, Y.-M.; Li, J., In Situ Observation of Random Solid Solution Zone in LiFePO<sub>4</sub> Electrode. *Nano Letters* **2014**, *14* (7), 4005-4010.
17. Li, Y., A review of recent research on nonequilibrium solid solution behavior in Li<sub>x</sub>FePO<sub>4</sub>. *Solid State Ionics* **2018**, *323*, 142-150.
18. Ulvestad, A.; Singer, A.; Clark, J. N.; Cho, H. M.; Kim, J. W.; Harder, R.; Maser, J.; Meng, Y. S.; Shpyrko, O. G., Topological defect dynamics in operando battery nanoparticles. *Science* **2015**, *348* (6241), 1344-1347.
19. Yu, Y.-S.; Kim, C.; Liu, Y.; van der Ven, A.; Meng, Y. S.; Kostecki, R.; Cabana, J., Nonequilibrium Pathways during Electrochemical Phase Transformations in Single Crystals Revealed by Dynamic Chemical Imaging at Nanoscale Resolution. *Advanced Energy Materials* **2015**, *5* (7), 1402040.
20. Orikasa, Y.; Maeda, T.; Koyama, Y.; Murayama, H.; Fukuda, K.; Tanida, H.; Arai, H.; Matsubara, E.; Uchimoto, Y.; Ogumi, Z., Direct Observation of a Metastable Crystal Phase of Li<sub>x</sub>FePO<sub>4</sub> under Electrochemical Phase Transition. *Journal of the American Chemical Society* **2013**, *135* (15), 5497-5500.
21. Zhang, X.; van Hulzen, M.; Singh, D. P.; Brownrigg, A.; Wright, J. P.; van Dijk, N. H.; Wagemaker, M., Rate-Induced Solubility and Suppression of the First-Order Phase Transition in Olivine LiFePO<sub>4</sub>. *Nano Letters* **2014**, *14* (5), 2279-2285.
22. Kobayashi, G.; Nishimura, S. i.; Park, M. S.; Kanno, R.; Yashima, M.; Ida, T.; Yamada, A., Isolation of Solid Solution Phases in Size-Controlled Li<sub>x</sub>FePO<sub>4</sub> at Room Temperature. *Advanced Functional Materials* **2009**, *19* (3), 395-403.
23. Furutsuki, S.; Chung, S.-C.; Nishimura, S.-i.; Kudo, Y.; Yamashita, K.; Yamada, A., Electrochromism of Li<sub>x</sub>FePO<sub>4</sub> Induced by Intervalence Charge Transfer Transition. *The Journal of Physical Chemistry C* **2012**, *116* (29), 15259-15264.

24. Rodríguez-Carvajal, J., Recent advances in magnetic structure determination by neutron powder diffraction. *Physica B: Condensed Matter* **1993**, *192* (1), 55-69.
25. Pigliapochi, R.; O'Brien, L.; Pell, A. J.; Gaultois, M. W.; Janssen, Y.; Khalifah, P.; Grey, C. P., When do Anisotropic Magnetic Susceptibilities Lead to Large NMR Shifts? Exploring Particle Shape Effects in the Battery Electrode Material LiFePO<sub>4</sub>. *Journal of the American Chemical Society* **2019**.
26. Hamelet, S.; Gibot, P.; Casas-Cabanas, M.; Bonnin, D.; Grey, C. P.; Cabana, J.; Leriche, J.-B.; Rodriguez-Carvajal, J.; Courty, M.; Levasseur, S.; Carlach, P.; Van Thournout, M.; Tarascon, J.-M.; Masquelier, C., The effects of moderate thermal treatments under air on LiFePO<sub>4</sub>-based nano powders. *Journal of Materials Chemistry* **2009**, *19* (23), 3979-3991.
27. Massiot, D.; Fayon, F.; Capron, M.; King, I.; Le Calvé, S.; Alonso, B.; Durand, J.-O.; Bujoli, B.; Gan, Z.; Hoatson, G., Modelling one- and two-dimensional solid-state NMR spectra. *Magnetic Resonance in Chemistry* **2002**, *40* (1), 70-76.
28. Cabana, J.; Shirakawa, J.; Chen, G.; Richardson, T. J.; Grey, C. P., MAS NMR Study of the Metastable Solid Solutions Found in the LiFePO<sub>4</sub>/FePO<sub>4</sub> System. *Chemistry of Materials* **2010**, *22* (3), 1249-1262.
29. Grey, C. P.; Dupré, N., NMR Studies of Cathode Materials for Lithium-Ion Rechargeable Batteries. *Chemical Reviews* **2004**, *104* (10), 4493-4512.
30. Rouse, G.; Rodriguez-Carvajal, J.; Patoux, S.; Masquelier, C., Magnetic Structures of the Triphylite LiFePO<sub>4</sub> and of Its Delithiated Form FePO<sub>4</sub>. *Chemistry of Materials* **2003**, *15* (21), 4082-4090.
31. Delmas, C.; Maccario, M.; Croguennec, L.; Le Cras, F.; Weill, F., Lithium deintercalation in LiFePO<sub>4</sub> nanoparticles via a domino-cascade model. *Nature Materials* **2008**, *7*, 665.
32. Cogswell, D. A.; Bazant, M. Z., Coherency Strain and the Kinetics of Phase Separation in LiFePO<sub>4</sub> Nanoparticles. *ACS Nano* **2012**, *6* (3), 2215-2225.
33. Singh, G. K.; Ceder, G.; Bazant, M. Z., Intercalation dynamics in rechargeable battery materials: General theory and phase-transformation waves in LiFePO<sub>4</sub>. *Electrochimica Acta* **2008**, *53* (26), 7599-7613.
34. Wang, L.; Zhou, F.; Meng, Y. S.; Ceder, G., First-principles study of surface properties of LiFePO<sub>4</sub>: Surface energy, structure, Wulff shape, and surface redox potential. *Physical Review B* **2007**, *76* (16), 165435.

35. Lepage, D.; Sobh, F.; Kuss, C.; Liang, G.; Schougaard, S. B., Delithiation kinetics study of carbon coated and carbon free LiFePO<sub>4</sub>. *Journal of Power Sources* **2014**, *256*, 61-65.
36. Liu, H.; Choe, M.-J.; Enrique, R. A.; Orvañanos, B.; Zhou, L.; Liu, T.; Thornton, K.; Grey, C. P., Effects of Antisite Defects on Li Diffusion in LiFePO<sub>4</sub> Revealed by Li Isotope Exchange. *The Journal of Physical Chemistry C* **2017**, *121* (22), 12025-12036.
37. Kuss, C.; Liang, G.; Schougaard, S. B., Atomistic modeling of site exchange defects in lithium iron phosphate and iron phosphate. *Journal of Materials Chemistry* **2012**, *22* (47), 24889-24893.
38. Ouvrard, G.; Zerrouki, M.; Soudan, P.; Lestriez, B.; Masquelier, C.; Morcrette, M.; Hamelet, S.; Belin, S.; Flank, A. M.; Baudalet, F., Heterogeneous behaviour of the lithium battery composite electrode LiFePO<sub>4</sub>. *Journal of Power Sources* **2013**, *229*, 16-21.

**For Table of Contents Only**

